LUNAR CARTOGRAPHY WITH THE APOLLO 17 ALSE RADAR IMAGERY*

M. TIERNAN, L. ROTH, T. W. THOMPSON, C. ELACHI, and W. E. BROWN, JR.

Space Sciences Division, Jet Propulsion Laboratory, California Institute of Technology, Pasadena, Calif., U.S.A.

(Received 12 July; in revised form 20 October, 1975)

Abstract. Lunar position differences between thirteen lunar craters in Mare Serenitatis were computed from VHF radar-imagery obtained by the Lunar Sounder instrument flown on the Apollo 17 Command Module. The radar-derived position differences agree with those obtained by conventional photogrammetric reductions of Apollo metric photography. This demonstrates the feasibility of using the Apollo Lunar Sounder data to determine the positions of lunar features along the Apollo 17 orbital tracks. This will be particularly useful for western limb and farside areas, where no Apollo metric camera pictures are available.

1. Introduction

Planetary surfaces are usually mapped from photographs taken from an orbiting spacecraft. Cartographic information of similar detail may be obtained from orbiting imaging radars which provide their own energy source and thus are not limited by cloud cover or solar illumination. Therefore, the radar extends the capabilities of optical camera mapping to areas which cannot be completely photographed with

TABLE I

DMA selenodetic coordinates of the 13 test craters

Crater	Latitude	Longitude
1	20°54′16″.971	26°11′17″.099
2	21°03′29″.635	25°30′16″.440
3	21°07′28″.914	25°16′21″.395
4	20°49′25″.207	22°43′15″.741
5	20°50′20″.431	22°43′15″.741
6	20°58′13″.694	20°27′01″.577
7	20°43′34″.696	19°44′54″.179
8	20°56′13″.192	19°46′01″.289
9	20°59′00″.449	19°09′53″.305
10	20°44′47″.343	16°09′48″.974
11	20°50′46″.347	15°49′41″.834
12	20°41′49″.040	15°47′44″.998
13	20°57′56″.046	14°19′17″.510

* This paper presents the results of one phase of research carried out at the Jet Propulsion Laboratory, California Institute of Technology, under Contract No. NAS 7-100, sponsored by the National Aeronautics and Space Administration.

sufficiently high resolution during a given mission such as the farside of the Moon, or cannot be photographed at all such as the surface of Venus.

Radar imagery of the lunar surface obtained from the Apollo 17 Lunar Sounder Experiment (ALSE) (Brown, 1972; Porcello *et al.*, 1974) provided the data for this study. A 30-kilometer-wide swath twice around the Moon was obtained during revs. 25 and 26. Thirteen one-kilometer-sized craters in the southern portion of Mare Serenitatis were chosen as test features (Figure 1, Table I). We calculated their positions from the ALSE imagery, for both orbits, and compared our results with positions calculated by the Defense Mapping Agency (Schimerman, 1974) based on photographs taken from the Apollo 17 metric camera. For the thirteen craters, the differences between the radar measurements and the DMA measurements had a mean of 0″.68 with a standard deviation of 25″.43 in longitude and a mean of 0″.90 with a standard deviation of 31″.24 in latitude. According to these results, it can be asserted that the

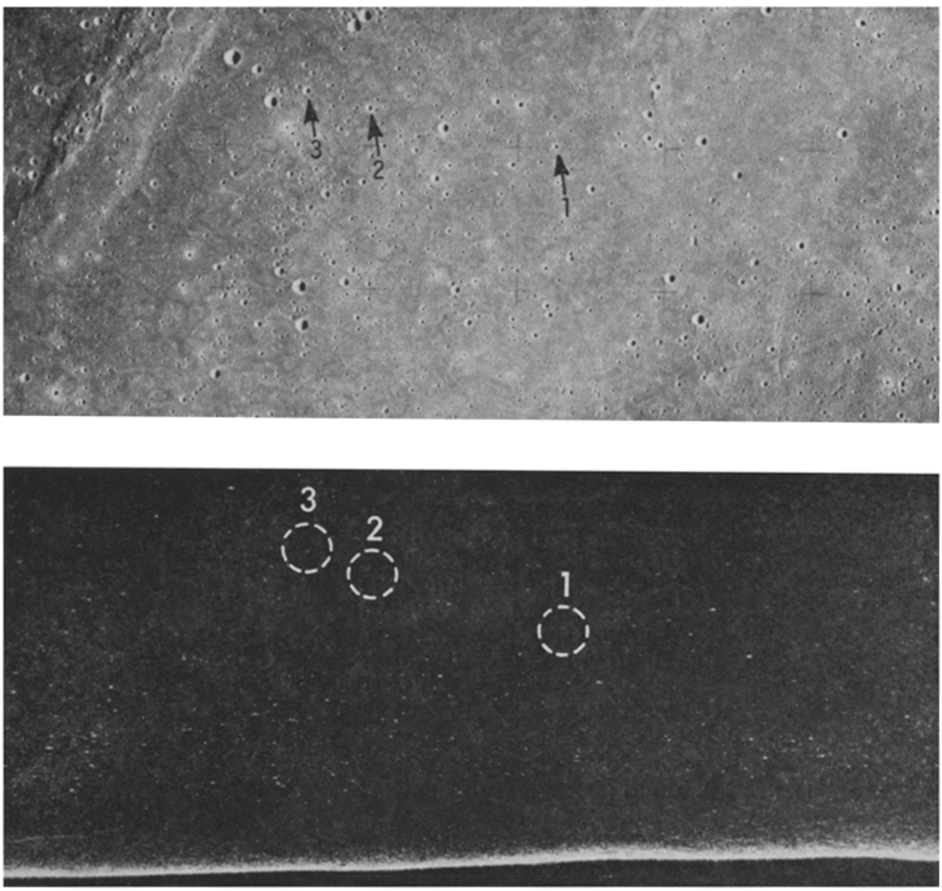

Fig. 1a. Photo and radar image of the craters 1, 2 and 3 in southern Mare Serenitatis. In this imagery east is to the left and north to the top of the page. The bright line corresponds to the nadir echo, i.e., first echo which is reflected by the nearest lunar point to the spacecraft.

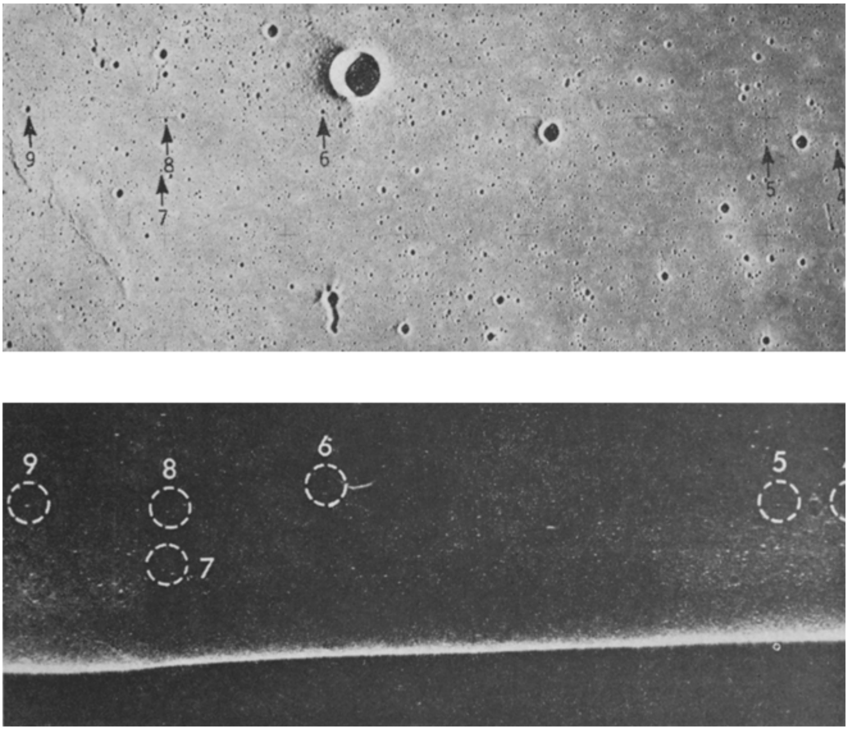

Fig. 1b. Photo and radar image of the craters 4 through 9 in southern Mare Serenitatis.

radar data can be used to complement the Apollo metric camera data, thus presenting the possibility of an extension of the Apollo photo position control net around the Moon.

2. Data Reduction Technique

Mapping based on photogrammetric techniques is a problem in projective geometry in which positions on the pictures are transformed into positions on the surface. On the radar imagery, however, distances between objects represent differences in time delays relative to the receiving antenna, thus necessitating a form of analysis different from conventional photogrammetric data reduction. Figure 2 shows the Apollo 17 imaging radar geometry. The along-track scale (X-axis) is linear in the radar image, whereas the crosstrack (Y-axis) is nonlinearly compressed: this results from the radar directly measuring the distance from the spacecraft to a specific surface feature (slant range).

The mathematical problem of computing differences in lunar positions from the radar data is a two-step process. The cross-track distance between a lunar feature and the spacecraft track is determined from the difference in range between the feature image and the bright nadir echo (Figure 1). The along-track distance is derived from the actual distance on the image, the spacecraft velocity, and the film running speed.

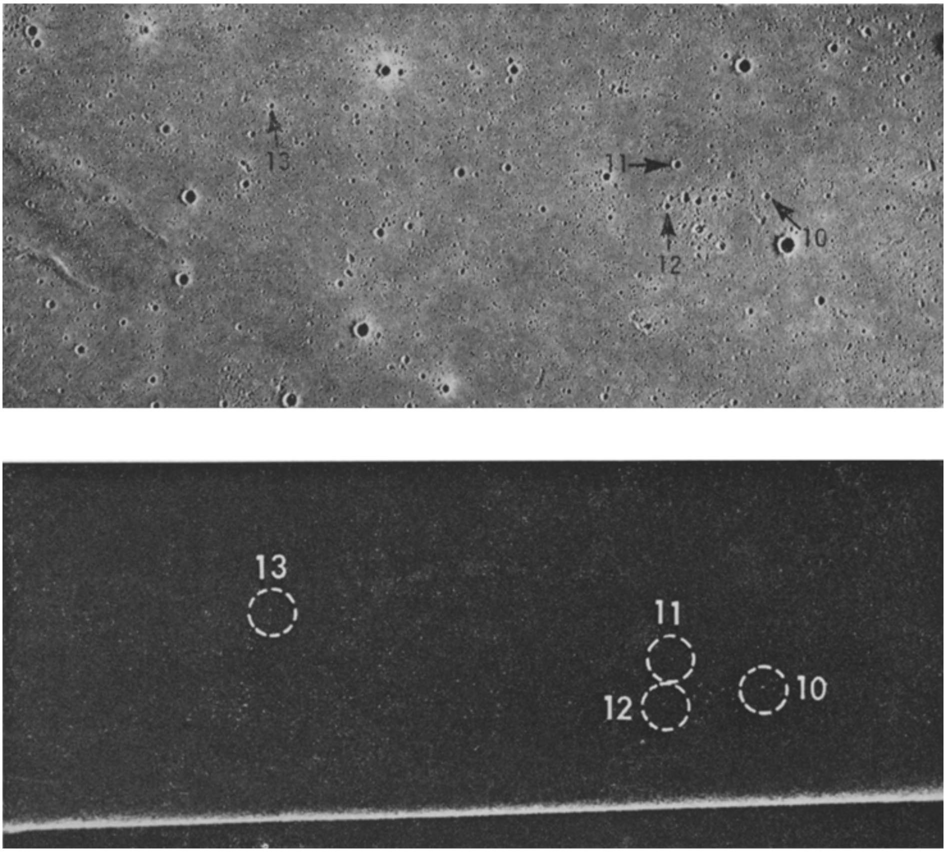

Fig. 1c. Photo and radar image of the craters 10 through 13 in southern Mare Serenitatis.

It is convenient to first compute the angular differences as seen from the center of mass of the Moon. Once these angular differences are known, a simple rotation gives the desired differences in latitude and longitude.

In the cross-track plane, the geometry indicates that the angle between the spacecraft and the point being measured, as seen from the lunar center of mass, is (Figure 2c)

$$\phi_i = \cos^{-1}\left[1 - \frac{Y_i}{2L_i}\left(\frac{Y_i + 2A_i}{L_i + A_i}\right)\right], \tag{1}$$

with

$$Y_i = y_i \frac{CK}{2}, \tag{2}$$

$$L_i = R + (H_i - A_i) = \text{local lunar radius to sub-satellite point} \tag{3}$$

where

R = radius of a reference sphere centered at the lunar center of mass (R = 1734.53 km, from the ephemeris);

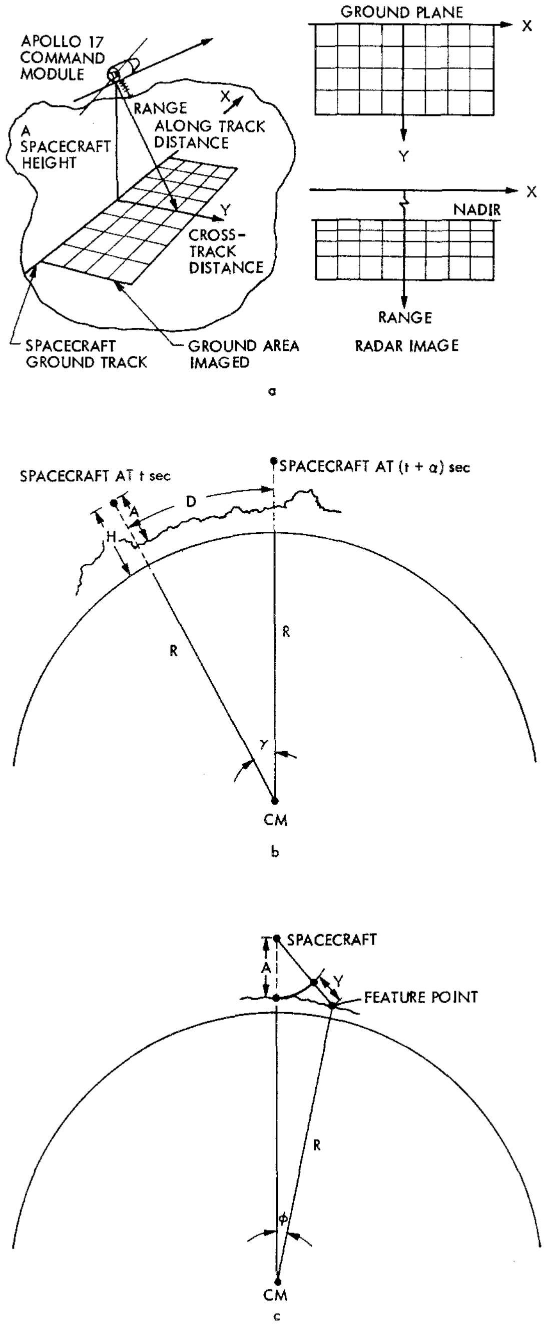

Fig. 2. Radar geometry. (a) the radar imagery covers a 30 km swath twice around the Moon. The radar measures time delay in range, therefore the image is nonlinearly compressed. (b) Along track geometry (orbit in the plane of the figure). (c) Cross track geometry (orbit perpendicular to the plane of the figure).

H_i = height of the spacecraft above the reference sphere;
C = speed of light;
K = known scaling factor which relates the distance across the film in millimeters to the time delay in seconds;
y_i = distance on the film between the bright nadir line and i the point being measured;
A_i = spacecraft height over the actual surface. This was determined from the time delay of the nadir echo.

In the along-track plane, the lunar center of mass being used as the origin, the angular distance γ_{ij} between two points is derived from the velocity of the spacecraft V and its distance $R+h_{ij}$ to the center of mass as

$$\gamma_{ij} = D/(R + h_{ij}), \qquad h_{ij} = (H_i + H_j)/2, \qquad D = VT,$$

where T is the flight time between two points and V is the spacecraft velocity. The value of T was determined by measuring the actual distance along the film between the points and multiplying it by an along-track scaling factor (s mm^{-1}) derivable from timing mark calibrations on the radar imagery. The above relations are valid for the case where the points i and j are relatively close. In other cases the relative angular distance must be divided into smaller sections.

Once the angular distances between points i and j ($\phi_{ij} = \phi_i - \phi_j$ and γ_{ij}) are known in the radar coordinates (Figure 2), and knowing the local angle of the ground track I_{ij}, relative to the lunar lines of latitude, we can derive the changes in latitude β_{ij} and longitude α_{ij} between the two points: i.e.,

$$\beta_{ij} = \sin^{-1}[\sin\delta \sin(\zeta + I_{ij})], \tag{4}$$

$$\alpha_{ij} = \cos^{-1}[\cos\delta/\cos\phi_{ij}], \tag{5}$$

where

$$\zeta = \sin^{-1}[\sin\gamma_{ij}/\sin\delta] \quad \text{and} \quad \delta = \cos^{-1}[\cos\gamma_{ij}/\cos\phi_{ij}].$$

3. Results and Error Analysis

Tables II and III present the relative longitude and latitude between 2 craters i and j obtained from our measurements and compare them with DMA photogrammetric measurements. For the longitude calculations, D_N had a mean of 0".7 with a standard deviation of 25".4; the ratio of D_N to the DMA measurement had a mean of 2.3% and a standard deviation of 8.4%. The mean of the latitude calculations was 0".9 with a standard deviation of 31".2. The ratio of D_N over the DMA measurement had a mean of 5.5% with a standard deviation of 19%. Our measurements of the local lunar radius (L_i, in Table IV) differ from DMA results by an average of 370 m (i.e., ~0.02%). In Table V, we present the relative difference in our measurements from one orbit to the next. In latitude this difference had a mean of −5".8 with a standard deviation of 16".3; for the longitude the mean was 2".7 with a standard deviation of 14".6.

The internal consistency of the results as evidenced by these numbers indicates that the inherent accuracy limit of the data has not been reached and that data external to the radar are the major sources of our differences with the DMA results. One major source of error has been the uncertainty in the exact positioning of the timing marks and thus a consequent inability to interpolate to intermediate times. This inability essentially quantizes the possible results for I_{ij}. Additionally, the limits of accuracy of the emphemeris preclude the possibility of determining more precisely the along-track scaling parameter, which again gives a quantizing effect that is noticeable in the data. If we ignore all crater pairs 2′ or less apart in latitude or longitude, then for the longitude results, the D_N to DMA ratio changes such that it has a mean of −0.02% with a standard deviation of 1.40%, and similarly the mean latitude D_N to DMA ratio becomes 1.00% with a standard deviation of 3.80%.

TABLE II

Longitude measurements

Craters (ij)	Photo	Radar (rev. 25)	D_{25}	Radar (rev. 26)	D_{26}
2–1	41′0″.659	41′18″.409	17″.750	[a]	–
3–1	54′55″.704	55′16″.025	20″.321	54′50″.754	−5″.130
4–3	2°33′05″.654	2°33′43″.749	38″.095	2°33′39″.413	33″.759
5–4	18′59″.890	18′58″.591	−1″.299	19′0″.421	0″.531
6–5	1°57′14″.274	1°56′47″.007	−27″.264	1°56′47″.796	−26″.478
8–6	41′0″.286	40′48″.133	−12″.153	40′51″.495	−8″.791
7–8	1′07″.110	1′32″.562	25″.452	1′18″.041	10″.931
9–7	35′0″.874	34′01″.542	−59″.332	34′29″.204	−31″.670
10–9	3°0′04″.331	3°0′44″.299	33″.968	3°0′42″.571	38″.240
11–10	20′07″.140	19′55″.939	−11″.201	19′31″.333	−35″.807
12–11	1′56″.836	2′02″.550	5″.714	1′57″.977	10″.141
13–12	1°28′27″.488	1°28′22″.974	−4″.514	1°28′34″.866	07″.378

$D_N \equiv$ Photo – radar (orbit N).
[a] Not identified on orbit 26.

TABLE III

Latitude measurements

Craters (i–j)	DMA	Radar (rev. 25)	D_{25}	Radar (rev. 26)	D_{26}
2–1	9′12″.664	9′55″.302	42″.638	[a]	–
3–1	13′11″.943	14′03″.956	52″.013	14′26″.166	1′14″.223
4–3	18′03″.707	17′44″.029	−19″.678	17′50″.877	−12″.820
5–4	0′55″.224	0′44″.158	−11″.066	0′31″.893	−23″.331
6–5	7′53″.623	7′24″.337	−29″.287	7′53″.182	−0″.441
8–6	2′0″.52	1′20″.558	−39″.944	0′58″.175	−1′02″.327
7–8	12′38″.496	12′35″.570	−02″.926	12′33″.037	− 5″.459
9–7	15′25″.753	15′48″.610	22″.857	15′51″.472	25″.719
10–9	14′13″.106	14′25″.499	12″.393	15′0″.142	47″.036
11–10	5′59″.004	5′51″.200	−07″.804	5′58″.304	−0″.700
12–11	8′57″.307	9′01″.701	04″.394	9′01″.350	04″.043
13–12	16′13″.006	15′49″.242	−23″.764	15′52″.857	−25″.149

$D_N \equiv$ Photo – radar (orbit N).
[a] Not identified on orbit 26.

TABLE IV

Radius vectors (km)

Crater	Radar (rev. 25)	Radar (rev. 26)	Photo (DMA)
1	1734.749	1734.806	1734.415
2	1734.942	[a]	1734.506
3	1734.986	1734.935	1734.510
4	1735.027	1735.033	1734.612
5	1734.982	1734.976	1734.600
6	1934.910	1734.958	1734.657
7	1735.043	1735.132	1734.670
8	1735.041	1735.125	1734.686
9	1735.103	1735.026	1734.784
10	1735.124	1735.060	1734.725
11	1735.061	1735.123	1734.743
12	1735.079	1735.136	1734.737
13	1735.036	1735.104	1734.752

[a] Not identified on orbit 26.

TABLE V

Relative measurement error

Craters (*i*–*j*)	D_{LA}	D_{LO}
3–1	−22″.210	25″.451
4–3	−06″.848	04″.336
5–6	12″.065	−01″.830
6–5	−28″.845	−0″.786
8–6	22 383	−03″.362
7–8	02″.533	14″.521
9–7	−02″.862	−27″.662
10–9	−34″.643	01″.728
11–10	−07″.104	24″.606
12–11	0″ 50	04″.573
13–12	01″.385	−11″.892

D_{LA} ≡ orbit 25 latitude − orbit 26 latitude.
D_{LO} ≡ orbit 25 longitude − orbit 26 longitude.

The 13 craters selected for this study were all chosen in a relatively flat area. In the case of a rugged region, a third parameter, the height difference, has to be derived. This would require the use of data from both orbits simultaneously as a stereographic pair.

4. Conclusions

The ALSE radar imagery can be used to determine the relative location of features from an orbiting platform. The radar approach appears to be the only one which can extend the precision of the camera mapping to lunar areas presently not photographed to sufficiently high resolution.

The errors that seem to most greatly affect our accuracy can be significantly reduced by improved data processing techniques and it is possible to increase the accuracy of the external data, thus reducing quantization effects. So, though our analysis was limited to a local smooth area, this same procedure offers the opportunity to extend the Apollo photo grammetric position control net around the Moon. In rough terrain the accuracy with which the relative position of two points can be determined will be lower. However in that case, stereo measurements from two different orbits would still result in reasonable accuracy. In a recent paper, Leberl (1976) showed that position accuracy better than 400 m can be achieved with single radar imagery in 100 m rms rough terrain. In rougher terrain, similar accuracy can be achieved by stereo-radargrammetry.

Acknowledgements

We would like to thank the Defense Mapping Agency and in particular, Mr Lawrence Schimerman for his time and assistance in providing the photographic measurements. We also thank the NASA Lunar Program Office, especially Mr R. Bryson, for their support during this work.

References

Brown, W. E.: 1972, *Moon* **4**, 113.
Leberl, F.: 1976, paper submitted to *J. Geophys. Res.*
Porcello, L., Jordan, R. L., Zelenka, J. S., Adams, G. F., Phillips, R. J., Brown, W. E., Ward, S. H., and Jackson, P. L.: 1974, *Proc. IEEE* **62**, 769.
Schimerman, L.: 1974, personal communication.